Journal of Coordination Chemistry

ISSN: 0095-8972 (Print) 1029-0389 (Online) Journal homepage: http://www.tandfonline.com/loi/gcoo20

Synthesis, characterization, crystal structure, and antimicrobial studies of novel thiourea derivative ligands and their platinum complexes

Ummuhan Solmaz, Ilkay Gumus, Gun Binzet, Omer Celik, Gulten Kavak Balci, Aylin Dogen & Hakan Arslan

To cite this article: Ummuhan Solmaz, Ilkay Gumus, Gun Binzet, Omer Celik, Gulten Kavak Balci, Aylin Dogen & Hakan Arslan (2018) Synthesis, characterization, crystal structure, and antimicrobial studies of novel thiourea derivative ligands and their platinum complexes, Journal of Coordination Chemistry, 71:2, 200-218, DOI: 10.1080/00958972.2018.1427233

To link to this article: https://doi.org/10.1080/00958972.2018.1427233

JOURNAL OF COORDINATION CHEMISTRY, 2018
VOL. 71, NO. 2, 200–218
https://doi.org/10.1080/00958972.2018.1427233

Taylor & Francis
Taylor & Francis Group

Synthesis, characterization, crystal structure, and antimicrobial studies of novel thiourea derivative ligands and their platinum complexes

Ummuhan Solmaz[a], Ilkay Gumus[a], Gun Binzet[b], Omer Celik[c], Gulten Kavak Balci[c], Aylin Dogen[d] and Hakan Arslan[a]

[a]Faculty of Arts and Science, Department of Chemistry, Mersin University, Mersin, Turkey; [b]Faculty of Education, Department of Chemistry, Mersin University, Mersin, Turkey; [c]Science and Technology Applied and Research Center, Dicle University, Diyarbakır, Turkey; [d]Faculty of Pharmacy, Department of Pharmaceutical Microbiology, Mersin University, Mersin, Turkey

ABSTRACT

N,N-Di-*R*-*N*′-(4-chlorobenzoyl)thiourea (Di-*R*: diethyl, di-*n*-propyl, di-*n*-butyl and diphenyl) ligands (HL^{1-4}) and their Pt(II) complexes (*cis*-[$Pt(L^{1-4}\text{-}S,O)_2$]) have been synthesized and structurally characterized by elemental analyses, FT-IR and NMR spectroscopy. HL^2 ligand and *cis*-[$Pt(L^4\text{-}S,O)_2$] metal complex have been also characterized by a single-crystal X-ray diffraction study. HL^2, $C_{14}H_{19}ClN_2OS$, crystallizes in the monoclinic space group $P2_1/n$ (no. 14), with $Z = 4$, and unit cell parameters, $a = 11.1405(16)$ Å, $b = 9.7015(12)$ Å, $c = 14.790(2)$ Å, $\beta = 106.547(7)°$. The *cis*-[$Pt(L^4\text{-}S,O)_2$], $C_{40}H_{28}Cl_2N_4O_2PtS_2$: triclinic, space group *P*-1 (no. 2), $a = 8.9919(3)$ Å, $b = 14.7159(6)$ Å, $c = 15.7954(6)$ Å, $\alpha = 113.9317(18)°$, $\beta = 97.4490(18)°$, and $\gamma = 105.0492(16)°$. Single crystal analysis of complex, *cis*-[$Pt(L^{1-4}\text{-}S,O)_2$], revealed that a square planar coordination geometry is formed around the platinum atom by two sulfur and two oxygen atoms of the related ligands, which are in a *cis* configuration. In addition, the thiourea derivative ligands and their complexes were evaluated for both their *in-vitro* antibacterial and antifungal activity. The results have been reported, explained, and compared with fluconazole and ampicillin, used as reference drugs.

ARTICLE HISTORY
Received 17 February 2017
Accepted 23 December 2017

KEYWORDS
Benzoyl thiourea; platinum complex; antimicrobial activity; intermolecular interaction; crystal structure analysis

CONTACT Ilkay Gumus ilkay.gumus@mersin.edu.tr
Supplemental data for this article can be accessed at https://doi.org/10.1080/00958972.2018.1427233.

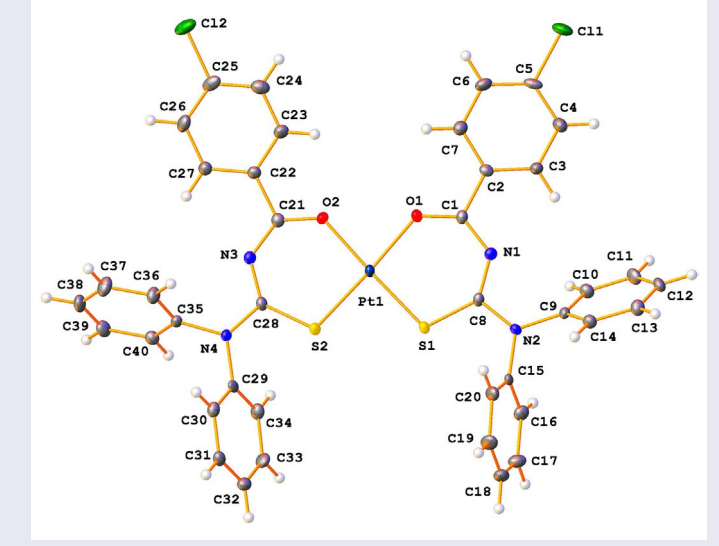

1. Introduction

Thiourea derivatives are a well-known class of significant ligands and able to bind to metal ions as neutral, monobasic, or dibasic ligands that have three potential donor atoms (N, O, and S) in complexation reactions [1–3]. In particular, benzoyl thioureas react with transition metal centers, either in monoanionic bidentate form by deprotonation, forming neutral homoleptic complexes with S, O and N, S coordination, or in neutral form only through S atom [4, 5]. Interest in thiourea derivatives and their metal complexes has increased due to the diversity of coordination and varied applications such as in precious metal separation and extraction [6], single source precursors for nanomaterials [7], plant growth regulator and biological activity, including antibacterial, anti-fungal, antitubercular, antithyroid, anti-helmintic, rodenticidal, insecticidal, herbicidal, *etc.* [8–17].

Thiourea ligands, which are selective ligands for the platinum group metals, have a strong affinity toward the platinum(II) center, which is coming from the sulfur atom. Thiourea derivatives can be acceptable as convenient sulfur-containing nucleophiles in order to react relatively fast with platinum(II) species in experiments, such as glutathione, which is present in biological systems [18, 19]. More recently, there have been efforts to design platinum-acylthiourea complexes in order to investigate their antifungal activity and inhibitory activities against viruses [20].

The prominence of such studies is the possibility that thiourea derivatives may be more effective as antimicrobial agents. However, there is a need for a comprehensive investigation relating to the structure and activity of thiourea derivatives as well as their stability under biological conditions. These detailed investigations could be helpful in the design of more potent antimicrobial agents. Based upon literature research, we could find no synthesis or characterization of the title compound type thiourea derivative metal complexes. In an effort to contribute to these studies, here we report the synthesis, characterization and antimicrobial properties of new *N,N*-di-R-*N*′-(4-chlorobenzoyl) thiourea ligands and their platinum metal complexes.

2. Experimental

2.1. Instrumentation

Melting points were recorded on an Electrothermal model 9200 apparatus. Carbon, hydrogen, and nitrogen analyses were carried out on a Carlo Erba MOD 1106 elemental analyzer. Infrared measurements were recorded from 400 to 4000 cm^{-1} on a Perkin Elmer Spectrum 100 series FT-IR/FIR/NIR Spectrometer Frontier, ATR instrument. The NMR spectra were recorded in $CDCl_3$ solvent on a Bruker Avance III 400 MHz NaNoBay FT-NMR spectrophotometer using tetramethylsilane as an internal standard.

The X-ray diffraction data were recorded on a Bruker APEX-II CCD diffractometer. A suitable crystal was selected and coated with Paratone oil and mounted onto a Nylon loop on a Bruker APEX-II CCD diffractometer. The crystal was kept at $T = 100$ K during data collection. The data were collected with MoKα ($\lambda = 0.71073$ Å) radiation at a crystal-to-detector distance of 40 mm. Using Olex2 [21], the structure was solved with the Superflip [22–24] structure solution program using the Charge Flipping solution method and refined by full-matrix least-squares on F^2 using ShelXL [25] with refinement of F^2 against all reflections. Hydrogens were located by difference maps and were refined isotropically, and all non-hydrogen atoms were refined anisotropically. The molecular structure plots were prepared using PLATON [26]. Geometric special details: all e.s.d.'s (except the e.s.d. in the dihedral angle between two l.s. planes) are estimated using the full covariance matrix. The cell e.s.d.'s are taken into account individually in the estimation of e.s.d.'s in distances, angles, and torsion angles; correlations between e.s.d.'s in cell parameters are only used when they are defined by crystal symmetry. An approximate (isotropic) treatment of cell e.s.d.'s is used for estimating e.s.d.'s involving l.s. planes.

2.2. Reagents

Potassium tetrachloroplatinate(II) was purchased from Sigma Aldrich. 4-Chlorobenzoyl chloride, potassium thiocyanate, diethylamine, di-*n*-propylamine, di-*n*-butylamine, and diphenylamine were purchased from Merck and used as received. All other chemicals and solvents were obtained from commercial suppliers and used without purification.

2.3. General procedure for the synthesis of ligands

$HL^{1–4}$ ligands were prepared according to previously published methods [27–29]. A solution of 4-chlorobenzoyl chloride (5 mmol, 0.860 g) in dry acetone (50 mL) was added dropwise to a suspension of potassium thiocyanate (5 mmol, 0.49 g) in acetone (30 mL). The reaction mixture was heated under reflux for 30 min and then cooled to room temperature. A solution of secondary amine (5 mmol, diethylamine: 0.370 g; di-*n*-propylamine: 0.510 g; di-*n*-butylamine: 0.650 g; diphenylamine: 0.850 g) in acetone (10 mL) was added and the resulting mixture was stirred for 2 h. Afterward, the reaction mixture was poured into hydrochloric acid (0.1 M, 300 mL) and the solution filtered. The solid product was washed with water and purified by recrystallization from an ethanol:dichloromethane mixture (1:1, *v*:*v*) (Scheme 1).

2.3.1. N,N-Diethyl-N′-(4-chlorobenzoyl)thiourea (HL^1)

Color: White. Yield: 80% (1.083 g). m.p.: 153–155 °C. FT-IR (ATR, *v*, cm^{-1}): *v*(N–H) 3274 (w); *v*(C–H) 2979, 2934, 2875 (w); *v*(C=O) 1642 (s); *v*(C=S) 1228 (s); *v*(C–Cl) 753 (w). ^{1}H NMR

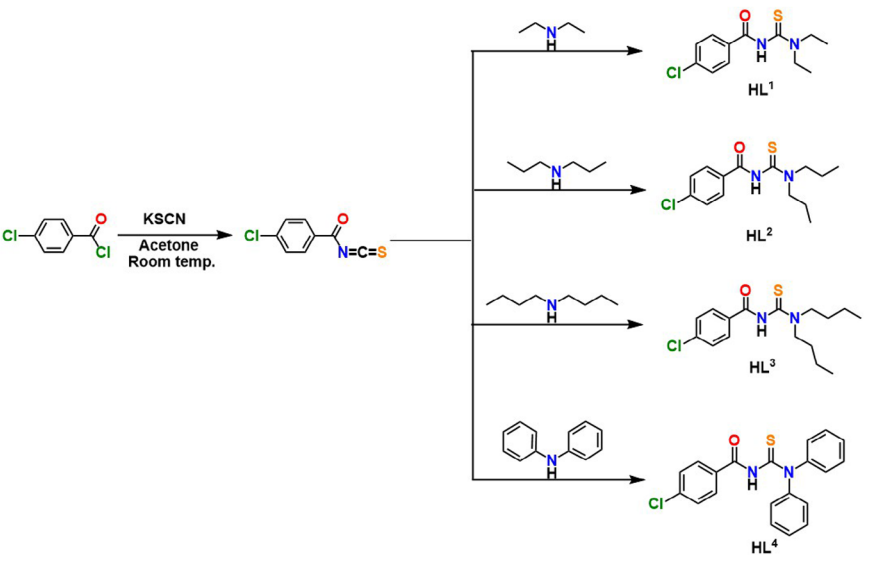

Scheme 1. Synthesis reaction of the ligands.

(400 MHz, $CDCl_3$, δ, ppm): 8.52 (s, 1H, NH), 7.78 (d, 2H, Ar–H), 7.44 (d, 2H, Ar–H), 4.02 (s, 2H, N–CH_2), 3.59 (s, 2H, N–CH_2), 1.33 (d, 6H, CH_3). ^{13}C NMR (100 MHz, $CDCl_3$, δ, ppm): 179.19 (C=S), 163.00 (C=O), 139.27, 130.97 (C–Ar), 129.38 (C–Ar), 129.09 (C–Ar), 47.98 (C–N), 47.68 (C–N), 13.29 (CH_3), 11.47 (CH_3). Anal. Calcd for $C_{12}H_{15}ClN_2OS$: C, 53.23; H, 5.58; N, 10.35. Found: C, 53.19; H, 5.50; N, 10.25%.

2.3.2. N,N-Di-n-propyl-N′-(4-chlorobenzoyl)thiourea (HL^2)

Color: White. Yield: 75% (1.120 g). m.p.: 98–99 °C. FT-IR (ATR, ν, cm^{-1}): ν(N–H) 3270 (w); ν(C–H) 2967, 2932, 2876 (w); ν(C=O) 1640 (s); ν(C=S) 1212 (s); ν(C–Cl) 753 (w). ^{1}H NMR (400 MHz, $CDCl_3$, δ, ppm): 8.85 (s, 1H, NH), 7.79 (d, 2H, Ar–H), 7.41 (d, 2H, Ar–H), 3.91 (s, 2H, N–CH_2), 3.47 (s, 2H, N–CH_2), 1.82 (s, 2H, CH_2), 1.69 (s, 2H, CH_2), 1.01 (s, 3H, CH_3), 0.88 (s, 3H, CH_3). ^{13}C NMR (100 MHz, $CDCl_3$, δ, ppm): 179.88 (C=S), 162.97 (C=O), 132.02 (C–Ar), 131.41 (C–Ar), 129.55, 127.78 (C–Ar), 55.02 (C–N), 54.95 (C–N), 21.48 (CH_2), 19.75 (CH_2), 11.35 (CH_3), 11.30 (CH_3). Anal. Calcd for $C_{14}H_{19}ClN_2OS$: C, 56.27; H, 6.41; N, 9.37. Found: C, 56.25; H, 6.39; N, 9.31%.

2.3.3. N,N-Di-n-butyl-N′-(4-chlorobenzoyl)thiourea (HL^3)

Color: White. Yield: 80% (1.310 g). m.p.: 88–89 °C. FT-IR (ATR, ν, cm^{-1}): ν(N–H) 3153 (w); ν(C–H) 2959, 2932, 2871 (w); ν(C=O) 1682 (s); ν(C=S) 1240 (s); ν(C–Cl) 749 (w). ^{1}H NMR (400 MHz, $CDCl_3$, δ, ppm):8.57 (s, 1H, NH), 7.77 (d, 2H, Ar–H), 7.43 (d, 2H, Ar–H), 3.96 (s, 2H, N–CH_2), 3.51 (s, 2H, N–CH_2), 1.78 (s, 2H, CH_2), 1.65 (s, 2H, CH_2), 1.44 (s, 2H, CH_2), 1.28 (s, 2H, CH_2), 0.98 (s, 3H, CH_3), 0.90 (s, 3H, CH_3). ^{13}C NMR (100 MHz, $CDCl_3$, δ, ppm): 179.62 (C=S), 162.81 (C=O), 139.24 (C–Ar), 130.97 (C–Ar), 129.36 (C–Ar), 129.09 (C–Ar), 53.27 (C–N), 52.98 (C–N), 30.13 (CH_2), 28.41 (CH_2), 20.05 (CH_2), 13.87 (CH_2), 13.71 (CH_3). Anal. Calcd for $C_{16}H_{23}ClN_2OS$: C, 58.79; H, 7.09; N, 8.57. Found: C, 58.71; H, 6.89; N, 8.49%.

2.3.4. N,N-Diphenyl-N′-(4-chlorobenzoyl)thiourea (HL^4)

Color: White. Yield: 88% (1.610 g). M.p.: 161–162 °C. FT-IR (ATR, *v*, cm^{-1}): *v*(N–H) 3257 (w); *v*(C=O) 1645 (w); *v*(C=S) 1251 (w); *v*(C–Cl) 757(w). ^{1}H NMR (400 MHz, $CDCl_3$, *δ*, ppm): 8.72 (s, 1H, NH), 7.53 (t, 3H, Ar–H), 7.33 (m, 10H, Ar–H), 7.25 (d, 2H, Ar–H).^{13}C NMR (100 MHz, $CDCl_3$, *δ*, ppm): 182.26 (C=S), 161.53 (C=O), 145.62 (C–Ar), 141.89 (C–Ar), 139.52 (C–Ar), 131.82 (C–Ar), 131.07 (C–Ar), 130.42 (C–Ar), 129.35 (C–Ar), 129.16 (C–Ar), 129.12 (C–Ar), 128.86 (C–Ar), 127.58 (C–Ar), 126.84 (C–Ar), 121.01 (C–Ar), 117.83 (C–Ar). Anal. Calcd for $C_{20}H_{15}ClN_2OS$: C, 65.48; H, 4.12; N, 7.64. Found: C, 65.18; H, 4.36; N, 7.44%.

2.4. General procedure for the synthesis of complexes

A solution of $HL^{1–4}$ (2.0 mmol, HL^1: 0.541 g; HL^2: 0.598 g; HL^3: 0.654 g; HL^4: 0.734 g) in ethanol (50 mL) at 70 °C was added dropwise to a solution of potassium tetrachloroplatinate(II) (1.0 mmol, 0.416 g) in water (50 mL) at 70 °C. The reaction mixture was stirred for 30 min and then cooled to room temperature. A yellow–brown precipitate formed which was filtered off and recrystallized from ethanol:dichloromethane (2:1, *v*:*v*) (Scheme 2) [30, 31].

2.4.1. Bis[4-chloro-N-(diethylcarbamothioyl)benzamido-O,S]platinum(II), cis-[Pt(L^1-S,O)$_2$]

Color: Yellow. Yield: 81% (0.595 g). FT-IR (ATR, *v*, cm^{-1}): *v*(C–H) 2975, 2932, 2869 (w); *v*(C–N) 1577 (w); *v*(C–O) 1488 (vs); *v*(C–S) 1087 (s); *v*(C–Cl) 749 (w). ^{1}H NMR (400 MHz, $CDCl_3$, *δ*, ppm): 8.16 (d, 4H, Ar–H), 7.39 (d, 4H, Ar–H), 3.82 (q, 4H, N–CH_2), 3.77 (q, 4H, N–CH_2), 1.34 (t, 6H, CH_3), 1.28 (t, 6H, CH_3). ^{13}C NMR (100 MHz, $CDCl_3$, *δ*, ppm): 167.53 (C–S), 167.24 (C–O), 137.67 (C–Ar), 136.14 (C–Ar), 130.67 (C–Ar), 128.38(C–Ar), 47.12(C–N), 46.02 (C–N), 31.58 (CH_2), 22.64 (CH_2), 13.10 (CH_3), 12.40 (CH_3). Anal. Calcd for $C_{24}H_{28}Cl_2PtN_4O_2S_2$: C, 39.2; H, 3.8; N, 7.6. Found: C, 39.0; H, 3.8; N, 7.8%.

2.4.2. Bis[4-chloro-N-(di-n-propylcarbamothioyl)benzamido-O,S]platinum(II), cis-[Pt(L^2-S,O)$_2$]

Color: Yellow. Yield: 78% (0.623 g). FT-IR (ATR, *v*, cm^{-1}): *v*(C–H) 2962, 2927, 2868 (w); *v*(C–N) 1578 (w); *v*(C–O) 1487 (vs), *v*(C–S) 1088 (s), *v*(C–Cl) 750 (w). ^{1}H NMR (400 MHz, $CDCl_3$, *δ*, ppm): 8.15 (d, 4H, Ar–H), 7.39 (d, 4H, Ar–H), 3.72 (q, 4H, N–CH_2), 3.65 (q, 4H, N–CH_2), 1.80 (m, 4H, CH_2-CH_2), 1.71 (m, 4H, CH_2-CH_2), 0.99 (t,6 H, CH_3), 0.94 (t, 6H, CH_3).^{13}C NMR (100 MHz, $CDCl_3$, *δ*, ppm): 167.71 (C–S), 167.36 (C–O), 137.63 (C–Ar), 136.16 (C–Ar), 130.64 (C–Ar), 128.37 (C–Ar),

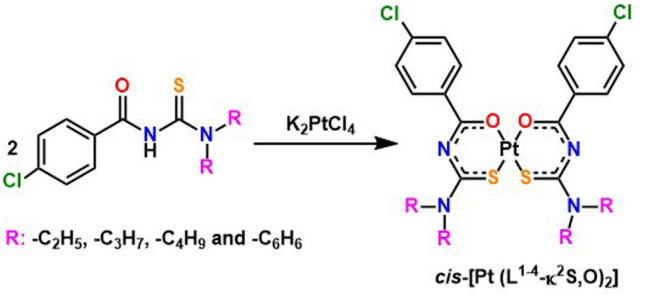

Scheme 2. Synthesis reaction of the complexes.

54.59 (C–N), 53.49 (C–N), 21.27 (CH_2), 20.50 (CH_2), 11.40 (CH_3). Anal. Calcd for $C_{28}H_{36}Cl_2PtN_4O_2S_2$: C, 42.5; H, 4.6; N, 7.1. Found: C, 41.6; H, 4.6; N, 7.3%.

2.4.3. Bis[4-chloro-N-(di-n-butylcarbamothioyl)benzamido-O,S]platinum(II), cis-[Pt(L^3-S,O)$_2$]

Color: Yellow. Yield: 67% (0.567 g). FT-IR (ATR, *v*, cm^{-1}): *v*(C–H) 2954, 2928, 2869 (w); *v*(C–N) 1600 (w); *v*(C–O) 1487 (vs); *v*(C–S) 1090 (s); *v*(C–Cl) 754 (w). ^{1}H NMR (400 MHz, $CDCl_3$, *δ*, ppm): 8.16 (d, 4H, Ar–H), 7.38 (d, 4H, Ar–H), 3.76 (q, 4H, N–CH_2), 3.68 (q, 4H, N–CH_2), 1.41 (m, 4H, CH_2-CH_2), 1.37 (m,4H, CH_2-CH_2), 0.98 (t,6H,CH_3), 0.94 (t, 6H, CH_3). ^{13}C NMR (100 MHz, $CDCl_3$, *δ*, ppm): 171.51 (C–S), 166.99 (C–O), 137.43 (C–Ar), 136.10 (C–Ar), 130.67 (C–Ar), 128.34 (C–Ar), 52.51 (C–N), 51.51 (C–N), 30.00 (CH_2), 29.26 (CH_2), 20.33 (CH_2), 13.80 (CH_3). Anal. Calcd for $C_{32}H_{44}Cl_2PtN_4O_2S_2$: C, 45.4; H, 5.2; N, 6.6. Found: C, 45.8; H, 5.3; N, 6.8%.

2.4.4. Bis[4-chloro-N-(diphenylcarbamothioyl)benzamido-O,S]platinum(II), cis-[Pt(L^4-S,O)$_2$]

Color: Brown. Yield: 79% (0.732 g). FT-IR (ATR, *v*, cm^{-1}): *v*(C–O) 1711, 1588 (s), *v*(C–S) 1085 (s), *v*(C–Cl) 843, 748 (s). ^{1}H NMR (400 MHz, $CDCl_3$, *δ*, ppm): 7.94 (d, 2H, Ar–H), 7.88 (d, 2H, Ar–H), 7.64 (t, 4H, Ar–H), 7.58–7.28 (m, 20H, Ar–H).^{13}C NMR (100 MHz, $CDCl_3$, *δ*, ppm): 167.21 (C–S), 166.83 (C–O), 142.62 (C–Ar), 141.53 (C–Ar), 137.50 (C–Ar), 129.84 (C–Ar), 129.07 (C–Ar), 128.35 (C–Ar), 128.01 (C–Ar), 127.36 (C–Ar), 127.14 (C–Ar), 126.83 (C–Ar), 126.51 (C–Ar), 126.01 (C–Ar), 119.01 (C–Ar), 117.03 (C–Ar). Anal. Calcd for $C_{40}H_{28}N_4O_2PtS_2$: C, 51.8; H, 3.0; N, 6.0. Found: C, 50.5; H, 3.2; N, 5.9%.

2.5. Cytotoxicity studies

To evaluate cytotoxicity, HEp-2 human cell line (ATCC CCL23) was selected. In preparation of the cell cultures, EMEM (Eagle's minimum essential medium) was used with 10% fetal bovine serum (Seromed) as growth medium. Incubation of the cells was performed in an atmosphere of 5% carbon dioxide at 37 °C. To determine the effects of the compounds on HEp-2 cells effects of added compound *versus* control cells with no added compound were observed. The nontoxic concentration was determined to be up to 1024 µg mL^{-1}. We used this limit in all experiments to test bacterial growth inhibition. In order to test the effects of the compounds on HEp-2 cells, 5×10^4 cells were seeded into each well of 12-well plates, cultured for 6 h at 28 °C, and allowed to grow for an additional 48 h in the presence of increasing amounts of compound (0.5, 1, 2, 4, 8, 16, 32, 64, 128, 256, 512, 1024 and 2048 µg mL^{-1}). Cytotoxicity of extracts was determined by a conventional haemocytometer using the trypan blue exclusion method [32–35]. The highest non-cytocidal (on HEp-2 cells) concentration of the chemical compounds was determined to be 1024 µg mL^{-1}. This limit was used for the determination of antimicrobial activities.

2.6. Antimicrobial activity studies

Antimicrobial susceptibility testing was performed by modification microdilution of the following literature methods [36, 37]. We used the microbial strains *Staphylococcus aureus* (ATCC 25923), *Streptococcus pneumonia* (ATCC 6303), *Escherichia coli* (ATCC 35218), *Pseudomonas aeruginosa* (ATCC 27853), *Acinetobacter baumannii* (RSHM 2026), *Candida albicans* (ATCC 10231), and *Candida glabrata* (RSHM 40199).

The fungal and bacterial cell inoculums were prepared from the stock culture grown in Tryptic Soy Agar (TSA) at 28 °C for 24 h and Mueller-Hinton Agar (MHA) 37 °C for 24 h, respectively. The micro-organism suspension concentrations were adjusted according to McFarland 0.5 turbidity tubes using sterilized saline. A stock solution of the title compound was prepared in DMSO at 1000 µg mL^{-1}. A modified microdilution test was applied for antimicrobial activity and the experiments were run in duplicates independently.

For antifungal activity testing, 100 µL of Tryptic Soy Broth (TSB) was added to each of 11 wells. 100 µL of chemical derivative solution was added to the first well and twofold dilutions were prepared. Then, 5 µL of fungal suspension was added to each tube except the last one, which acted as a control well.

For antibacterial activity testing, 100 µL of Mueller-Hinton Broth (MHB) was added to each of 11 wells. 100 µL of chemical derivative solution was added to the first tube and twofold dilutions were prepared. Then 5 µL of the bacterial suspension was added to each tube except the last control well. Only 5 µL of fungal and bacterial suspension were added in another control tube without chemical and used as a control for growing. All plates were incubated at 28 °C (for fungi) and at 37 °C (for bacteria) for 24 h. After the incubation, the minimal inhibitory concentrations (MIC) were noted by controlling the growth inhibition for title compound (Table 1). Fluconazole and ampicillin were used as reference drugs. The results were read visually and by measuring optical density for 24 h.

3. Results and discussion

3.1. Spectroscopic characterization of the ligand and platinum complexes

Ligands were synthesized in two steps. In the first step, 4-chlorobenzoyl isothiocyanate was synthesized by reaction of 4-chlorobenzoyl chloride with an equimolar amount of potassium thiocyanate in dry acetone. In the second step, ligands ($HL^{1–4}$) were obtained from reaction of 4-chlorobenzoyl isothiocyanate with a secondary amine (diethylamine, di-*n*-propylamine, di-*n*-butylamine, and diphenylamine) in dry acetone. Scheme 1 outlines the synthesis of the series of thiourea derivatives. The ligands were purified by recrystallization from an

Table 1. MIC values (µg mL^{-1}) of the ligands and metal complexes tested against the Gram-positive, Gram-negative bacterial and fungal and cytotoxicity values (µg mL^{-1}) against the HEp-2 human cell line.*

	Gram-positive bacteria		Gram-negative bacteria			Fungal		Cytotoxicity (µg mL^{-1})
Compound	*S. aureus*	*S. pneumoniae*	*A. baumannii*	*E. coli*	*P. aeruginosa*	*C. albicans*	*C. glabrata*	HEp-2
HL^1	62.50	15.62	15.62	15.62	15.62	31.25	31.25	1024
HL^2	62.50	7.80	7.80	62.50	7.80	31.25	31.25	1024
HL^3	31.25	31.25	31.25	125.00	31.25	31.25	31.25	2048
HL^4	31.25	31.25	31.25	31.25	31.25	31.25	31.25	1024
cis-$[Pt(L^1\text{-}S,O)_2]$	62.50	62.50	31.25	31.25	31.25	15.62	31.25	2048
cis-$[Pt(L^2\text{-}S,O)_2]$	15.62	3.90	3.90	15.62	3.90	62.50	62.50	2048
cis-$[Pt(L^3\text{-}S,O)_2]$	62.50	62.50	31.25	31.25	31.25	15.62	31.25	1024
cis-$[Pt(L^4\text{-}S,O)_2]$	62.50	62.50	15.62	31.25	31.25	125.00	250.00	2048
Fluconazole						–	–	
Ampicillin	–	–	–	31.25	31.25			
K_2PtCl_4	250	250	62.5	125	125	125	62.5	

*"–": Effective in all concentrations used.

ethanol:dichloromethane mixture and characterized by elemental analysis, ^{1}H NMR, ^{13}C NMR and FT-IR techniques. Data of all synthesized compounds confirm the proposed structures (Figures S1, S3, S7, S9, S11, S15, S17, S19, S23, Supporting Information). The reaction of the ligands with potassium tetrachloroplatinate(II) at room temperature with an ethanol:water mixture as solvent yielded the four new complexes *cis*-[Pt(L^{1-4}-S,O)$_2$] (Scheme 2). All the new metal complexes were recrystallized from an ethanol:dichloromethane mixture and characterized by elemental analysis, ^{1}H NMR, ^{13}C NMR, cozy, HMQC, and FT-IR techniques (Figures S2, S4, S5, 6S, S8, S10, S12, S13, S14, S16, S18, S20, S21, S22, and S24, Supporting Information). The proposed structures given in Schemes 1 and 2 are consistent with the analytical and spectroscopic data.

IR spectral analysis confirms the presence of characteristic groups in the prepared compounds. The main vibrational bands of the investigated compounds are given in the Experimental section. The IR spectra of all prepared ligands showed characteristic bands approximately at ~3200 cm^{-1} corresponding to a *ν*(NH) stretching vibration. This band disappears upon metal complex formation. The strong *ν*(C=O) stretching vibration bands for the free ligands were observed in the range of 1640–1681 cm^{-1}. In the obtained complexes, the *ν*(C=O) stretching vibration frequency decreases by ~155–195 cm^{-1}, in agreement with the literature [38]. A thiocarbonyl *ν*(C=S) vibration band appeared at 1212–1251 cm^{-1} for the free ligands. These bands shifted to lower values (~1085–1090 cm^{-1}) for complex compounds as a result of the coordination via sulfur and oxygen atoms to platinum ions (Figures S7, S8, S15, S20, and S23, Supporting Information). These results agree with the data supplied in the literature [38, 39].

The ^{1}H NMR spectra of the ligands were recorded in $CDCl_3$. The ^{1}H NMR data of the obtained compounds are given in the Experimental section and are consistent with the structural results. The signals belonging to the NH groups of the ligands were observed the most downfield as a singlet in the range of *δ* 8.51–8.85 ppm in the NMR spectra (Figures S1, S9, and S17, Supporting Information). But these signals did not appear in the ^{1}H NMR spectrum of the Pt(II) complexes (Figures S2, S10, and S16, Supporting Information). The signals for the aromatic protons in the free ligands were observed at *δ* ~7–8 ppm; slight variations were observed as a result of the difference in their environments. After complexation occurred, the aromatic proton resonance values for protons number 2,2′,4,4′ shifted downfield (Δ*δ* ~0.35 ppm). Protons number 1,1′,3,3′ are nearly identical (a slight difference in the shift of signals amounting to Δ*δ* ~0.05 ppm). In ^{1}H NMR spectra of the HL^{1-3} ligands, different ^{1}H resonances are observed for each of the two ethylene groups of the (S)CN(CH_2)$_2$- moiety at room temperature in $CDCl_3$ (*δ* 4.02 and 3.59 (for HL^{1}); *δ* 3.91 and 3.47 ppm (for HL^{2}); *δ* 3.96 and 3.51 ppm (for HL^{1}); *δ* 4.02 and 3.59 ppm (for HL^{3})). Since, the resonance in C(O)–NH–C(S)–N part gives the single bond a double bond character and slows the rotation of the C–N bond [40–45]. For HL^{1-3} ligands, this restricted rotation results interestingly in the formation of *E*/*Z* configurational isomerism in solution [43–45]. The coordination of Pt^{2+} with the ligands does not change the main profile of the ligands NMR signals of the chemical shifts of the two ethylene groups get closer, indicating that the anisotropy of the two ethyl groups is less (*δ* 3.82 and 3.77 (for HL^{1}); *δ* 3.72 and 3.65 ppm (for *cis*-[Pt(L^{1}-S,O)$_2$); *δ* 3.76 and 3.68 ppm (for *cis*-[Pt(L^{2}-S,O)$_2$); *δ* 4.02 and 3.59 ppm (for *cis*-[Pt(L^{3}-S,O)$_2$)). In other words, a significant consequence of complexation is an increase of the C–N rotation [43–45]. The most upfield protons in ^{1}H NMR spectra of all the ligands appear as one sharp triplet between *δ* 0.85–1.00 ppm which is generated by six protons assigned to -CH_3 groups of ligands. The other aliphatic

proton signals (–C<u>H</u>$_2$–CH$_3$, -C<u>H</u>$_2$–CH$_2$ and N–C<u>H</u>$_2$) of the free ligands are shown relatively in downfield. These resonance values for the complexes 1–3 are almost identical with a slight difference in the shift of signals (Figures S1, S2, S9, S10, S17, and S18, Supporting Information).

In ^{13}C NMR, the characteristic thiocarbonyl (C=S) and carbonyl (C=O) carbons for all free ligands appeared at δ 179–162 ppm range. The C=S and C=O carbon resonance values of the complexes shifted upfield ($\Delta\delta$ ~12 ppm) and downfield ($\Delta\delta$ ~5 ppm), respectively, when compared with the free ligand's resonances. Consequently, the shift of signals in NMR spectra of complexes, compared with free ligand, is the result of the complexation process.

3.2. Crystal structure description

Suitable crystals for X-ray analysis of HL^2 ligand were obtained upon slow diffusion of dichloromethane into an ethanolic solution of the ligand. HL^2 crystallizes in the monoclinic space group P2$_1$/n. The crystallographic data and structure refinement parameters are summarized in Table 2. Figure 1(a) shows an ORTEP III drawing and atom labeling, Figure 1(b) a packing diagram and Figure 1(c) intra- and intermolecular hydrogen bond interactions of the ligand.

Single crystal analysis of the ligand revealed that the conformation of the HL^2 with respect to the C=S and C=O groups is twisted, as seen by the torsion angles C8–N1–C1–O1 and C1–N1–C8–S1 of −12.0(2) and −109.53(14)°, forming weak C12–H12A···S1 3.080(2) Å intramolecular interactions. The dihedral angle between the O1–C1–N1 and S1–C8–N1 planes is 64.99°. The obtained bond lengths and angles for HL^2 are typical for thiourea derivatives; both C8-S1 (1.677(17) Å) and C1-O1 (1.221(2) Å) bonds show a typical double-bond character. Also, the C–N bond lengths in –C(O)–NH–C(S)–N part (C1–N1 1.385(2), N1–C8 1.414(2) and

Table 2. Crystal data and details of the structure refinement for HL^2 and *cis*-[Pt(L^4-S,O)$_2$].

Parameters/compound	HL^2	*cis*-[Pt(L^4-S,O)$_2$]
Crystal formula	$C_{14}H_{19}ClN_2OS$	$C_{40}H_{28}Cl_2N_4O_2PtS_2$
Formula weight	298.82	926.77
Crystal dimensions (mm)	0.26 × 0.22 × 0.22	0.23 × 0.1 × 0.04
Temperature (K)	100	100
Crystal system	Monoclinic	Triclinic
Space group	*P*2$_1$/n	*P*-1
a (Å)	11.1405(16)	8.9919(3)
b (Å)	9.7015(12)	14.7159(6)
c (Å)	14.790(2)	15.7954(6)
α (°)	90	113.9317(18)
β (°)	106.547(7)	97.4490(18)
γ (°)	90	105.0492(16)
Z	4	2
D_{calc} (g.cm^{-1})	1.295	1.731
Range of θ (°)	6.834–63.444	5.546–61.26
μ (mm^{-1})	0.380	4.256
Reflections collected	26,237	72,763
Index ranges	$-15 \le h \le 14$ $14 \le k \le 12$ $-21 \le l \le 21$	$-12 \le h \le 12$ $-21 \le k \le 20$ $-22 \le l \le 22$
Reflections used in refinement	4990	10,913
No. of refined parameters	194	460
Final *R* indexes [$I \ge 2\sigma(I)$]	$R_1 = 0.0494$ $wR_2 = 0.0918$	$R_1 = 0.0407$ $wR_2 = 0.0559$
Final *R* indexes [all data]	$R_1 = 0.0915$ $wR_2 = 0.1051$	$R_1 = 0.0702$ $wR_2 = 0.0616$
GOF	1.031	1.039
$(\Delta\rho)_{min}$–$(\Delta\rho)_{max}$ (e Å^{-3})	0.67, −0.70	1.10, −1.53

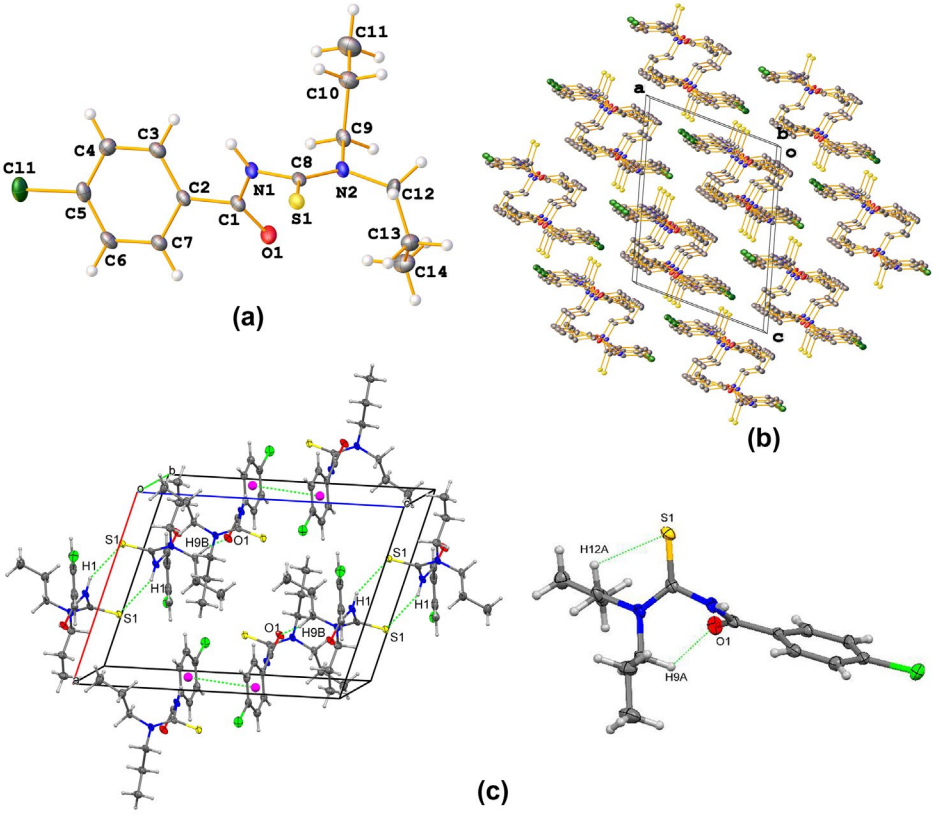

Figure 1. (a) ORTEP view of HL^2. (b) The crystal packing of HL^2. (c) The intramolecular hydrogen bond interactions (left), intermolecular hydrogen bond and $\pi\cdots\pi$ stacking interactions (right) are shown as green dashed lines in crystal packing of HL^2.

N2–C8 1.325(2) Å) are shorter than a normal single C–N bond length (1.469 Å), indicating a double bond character. Thus, hybridization on nitrogen atoms changes from sp^3 to sp^2. The main bond lengths of HL^2 are within the ranges obtained for similar compounds. These results are confirmed by bond angles and lengths (Table 3). There are no significant differences in the bond distances and angles comparing with other benzoylthioureas [32–35, 38, 39, 46].

In the ligand molecules, C9–H9A···O1 (D···A: 3.141(2) Å), C12–H12A···S1 (D···A: 3.080(2) Å) intramolecular interactions occur. These intramolecular hydrogen bonds in the ligand are shown as a light green dashed line in Figure 1(c). The molecules of ligand exhibit a characteristic intermolecular pattern, forming dimers via N–H···S (N1–H1···$S1^{i}$ (D···A: 3.4437(16) Å, (i) 1–*x*, 1–*y*, 2–*z*)) hydrogen bonding to give an eight-membered ring exhibiting an $R^2_2(8)$ hydrogen bonding motif. This intermolecular hydrogen bonding motif occurs between the thiocarbonyl sulfur atom and the hydrogen of the amide (Figure 1(c)). Also, the ligand molecules are connected to each other through intermolecular C6–H6···$S1^{ii}$ (D···A: 3.7859(18) Å, (ii) *x*, –1+*y*, *z*) hydrogen bonds and $\pi\cdots\pi$ stacking (3.721 Å, (i) 1–*x*, –*y*, 2–*z*). In the crystal structure, these intermolecular hydrogen bond interactions and $\pi\cdots\pi$ stacking allow clustering of molecules.

A yellow block-shaped crystal of *cis*-[Pt(L^{1-4}-S,O)$_2$] obtained from recrystallization in dichloromethane:ethanol (1:1, *v*:*v*) mixture was selected and the structure of the platinum complex was confirmed by the result of single crystal X-ray diffraction determination. The results confirmed the connectivity of the ligand to the metal as 2:1 and a square planar geometry around the metal center. Single crystal X-ray analysis shows *cis*-[Pt(L^4-S,O)$_2$] belongs to triclinic crystal system, space group *P*-1. The details of crystallographic data and structure refinement parameters are summarized in Table 2. Figure 2(a) shows an ORTEPIII drawing and atom labeling and Figure 2(b) a schematic of selected bond lengths (Å) for the studied complex, which is a *cis* form. The Pt ion lies on a crystallographic center of symmetry and has a slightly distorted square planar coordination with two S and O atoms at the corners of coordination. The coordination angle between O1–O2–Pt and Pt–S1–S2 planes is 0.44°. The Pt-S1, Pt–S2, Pt–O1, and Pt–O2 bond lengths are 2.2306(8), 2.2327(9), 2.027(2), and

Table 3. Selected bond lengths (Å), bond angles and torsion angles (°) for HL^2.

Distance (Å)		Bond angle (°)		Torsion angle (°)	
Cl1–C5	1.7392(17)	C1–N1–C8	119.29(13)	Cl1–C5–C6–C7	−178.22(12)
S1–C8	1.6773(17)	C8–N2–C9	123.31(14)	O1–C1–C2–C3	−145.18(17)
O1–C1	1.221(2)	C8–N2–C12	121.41(14)	O1–C1–C2–C7	32.2(2)
N1–C1	1.385(2)	C12–N2–C9	115.25(13)	N1–C1–C2–C3	34.0(2)
N1–C8	1.414(2)	O1–C1–N1	122.22(15)	N1–C1–C2–C7	−148.63(15)
N2–C8	1.325(2)	O1–C1–C2	121.92(14)	N2–C9–C10–C11	−179.52(15)
N2–C9	1.473(2)	N1–C1–C2	115.85(13)	N2–C12–C13–C14	−177.13(19)
N2–C12	1.465(2)	C3–C2–C1	122.61(14)	N2–C12–C13A–C14A	56.2(5)
C1–C2	1.487(2)	C3–C2–C7	119.78(15)	C1–N1–C8–S1	−109.53(14)
C2–C3	1.389(2)	C7–C2–C1	117.56(15)	C1–N1–C8–N2	69.86(19)
C2–C7	1.396(2)	C4–C3–C2	120.21(15)	C1–C2–C3–C4	177.20(15)
C3–C4	1.387(2)	C5–C4–C3	118.95(16)	C1–C2–C7–C6	−178.92(14)
C4–C5	1.383(2)	C4–C5–Cl1	119.63(14)	C2–C3–C4–C5	1.8(2)
C5–C6	1.386(2)	N1–C8–S1	118.93(11)	C3–C2–C7–C6	−1.5(2)
C6–C7	1.382(2)	N2–C8–S1	125.45(13)	C3–C4–C5–Cl1	176.65(13)
C9–C10	1.518(2)	N2–C8–N1	115.61(14)	C3–C4–C5–C6	−1.9(3)
C10–C11	1.521(3)	N2–C9–C10	110.51(13)	C8–N1–C1–O1	−12.0(2)
C12–C13	1.583(4)	C9–C10–C11	111.55(15)	C8–N1–C1–C2	168.83(14)
C12–C13A	1.455(6)	N2–C12–C13	104.82(16)	C8–N2–C9–C10	86.65(18)
C13–C14	1.514(4)	C13A–C12–N2	125.2(3)	C8–N2–C12–C13	95.85(19)
C13A–C14A	1.528(10)	C14–C13–C12	110.3(2)	C8–N2–C12–C13A	69.4(4)

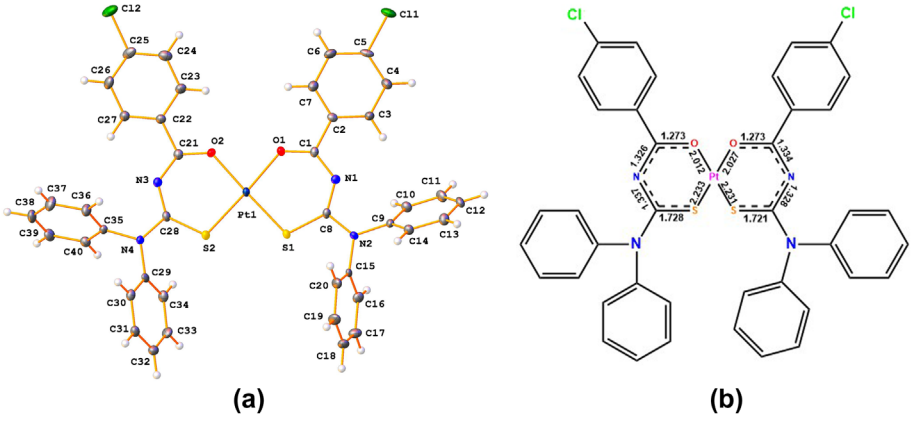

Figure 2. (a) ORTEP view of *cis*-[Pt(L^4-S,O)$_2$] with the atom numbering scheme. Displacement ellipsoids are shown at the 50% probability level. (b) Schematic of selected bond lengths (Å) in *cis*-[Pt(L^4-S,O)$_2$] complex.

2.012(2) Å, respectively. The small differences between the Pt–S1 and Pt–S2 bond lengths (2.2306(8) compared with 2.2327(9) Å) as well as between the Pt–O1 and Pt–O2 bond lengths (2.027(2) compared with 2.027(2) Å) lead to difference between the two chelate rings (Pt–S1–C8–N1–C–O1 and Pt–S2–C28–N3–C21–O2). These small differences are also reflected in the other pertinent bond lengths and angles. The origin of these small differences may be due to packing effects [47]. The bond angles of S1–Pt–S2, S1–Pt–O1, S1–Pt–O2, S2–Pt–O1, S2–Pt–O2, and O1–Pt–O2 are 87.66(3), 95.35(7), 177.85(7), 176.98(7), 94.46(7), and 82.53(9)°, respectively. These structural parameters imply a slightly distorted square planar geometry around the platinum center. Other values of bond angles and torsion angles are given in Table 4.

The double bond character of the carbonyl and thiocarbonyl groups when compared to literature results are weakened (C1–O1 1.273(4) and C21–O2 1.273(4) Å, C8–S1 1.721(3), C28–S2 1.728(3) Å) due to the donation of electrons to the metal center (Figure 2(b)). The bond lengths of all C–N bonds of synthesized *cis*-[Pt(L^4-S,O)$_2$] complexes (C1–N1 1.334(4), N1–C8 1.328(4), N3–C21 1.326(4), and N3–C28 1.337(4)) are shorter than the normal C–N single bond (1.48 Å) and longer than normal C=N double bond (1.25 Å). These results are in agreement with expected delocalization in the molecule and confirmed by C1–N1–C8–N2 and C21–N3–C28–N4 angles [30, 31, 46–54]. All other bond lengths are within normal range (Table 4).

The molecular geometry of *cis*-[Pt(L^4-S,O)$_2$] was affected by intra- and intermolecular hydrogen bond interactions. In addition, the crystal structure is further stabilized by C–H···Cg and Cg···Cg ($\pi\cdots\pi$) interactions (Tables 5 and 6), where Cg1 is the center of gravity of Pt(1)–S(1)–C(8)–N(1)–C(1)–O(1), Cg2 is the center of gravity of Pt(1)–S(2)–C(28)–N(3)–C(21)–O(2), Cg3 is the center of gravity of C2–C7, Cg4 is the center of gravity of C9–C14, Cg5 is the center of gravity of C15–C20, Cg6 is the center of gravity of C22–C27, Cg7 is the center of gravity of C29–C34 and Cg8 is the center of gravity of C35–C40. As shown in Figure 3, in the complex, intermolecular C–H···Cl, C–H···S and C–H···N hydrogen bond interactions occurs (C13–H13···Cl2^{i} 3.572(4) Å; C12–H12···Cl1^{ii} 3.434(3) Å; C11–H11···S1^{iii} 3.903(4) Å; C31–H31···S1^{iv}

Table 4. Selected bond lengths (Å), bond angles and torsion angles (°) for *cis*-[Pt(L^4-S,O)$_2$].

Distance (Å)		Bond angle (°)		Torsion angle (°)	
Pt1–S1	2.2306(8)	S1–Pt1–S2	87.66(3)	Pt1–S1–C8–N1	−4.8(4)
Pt1–S2	2.2327(9)	O2–Pt1–S1	177.85(7)	Pt1–S1–C8–N2	178.0(2)
Pt1–O2	2.012(2)	O2–Pt1–S2	94.46(7)	Pt1–S2–C28–N3	−8.4(4)
Pt1–O1	2.027(2)	O2–Pt1–O1	82.53(9)	Pt1–S2–C28–N4	172.9(2)
S1–C8	1.721(3)	O1–Pt1–S1	95.35(7)	Pt1–O2–C21–N3	−4.4(6)
S2–C28	1.728(3)	O1–Pt1–S2	176.98(7)	Pt1–O2–C21–C22	176.2(2)
Cl1–C5	1.737(3)	C8–S1–Pt1	107.49(11)	Pt1–O1–C1–N1	−4.2(5)
Cl2–C25	1.744(4)	C28–S2–Pt1	107.89(12)	Pt1–O1–C1–C2	174.6(2)
O2–C21	1.273(4)	C21–O2–Pt1	129.6(2)	S2–C28–N4–C35	166.2(2)
O1–C1	1.273(4)	C1–O1–Pt1	128.8(2)	S2–C28–N4–C29	−1.7(4)
N3–C28	1.337(4)	C21–N3–C28	126.5(3)	Cl1–C5–C4–C3	178.3(3)
N3–C21	1.326(4)	C8–N1–C1	127.5(3)	N3–C28–N4–C35	−12.7(5)
N1–C8	1.328(4)	C8–N2–C9	122.4(3)	N3–C28–N4–C29	179.5(3)
N1–C1	1.334(4)	C8–N2–C15	122.3(3)	N2–C9–C14–C13	177.7(3)
N2–C8	1.364(4)	C9–N2–C15	115.4(2)	N2–C9–C10–C11	−179.0(3)
N2–C9	1.440(4)	N1–C8–S1	130.7(2)	C8–N1–C1–O1	1.7(6)
N2–C15	1.446(4)	N1–C8–N2	114.4(3)	C8–N1–C1–C2	−177.2(3)
C28–N4	1.354(4)	N2–C8–S1	114.8(2)	C8–N2–C9–C14	124.4(3)
C9–C14	1.385(5)	N3–C28–S2	130.1(3)	C8–N2–C9–C10	−58.7(5)

Table 5. Geometrical parameters of C–H/Cl···π interactions for *cis*-[Pt(L^4-S,O)$_2$] (Å, °).

D–H···Cg	d(*D*–H)	d(H···*A*)	d(*D*···A)	∠(*D*–H···A)	d(H···Cg)
C30–H30···Cg(1)^{i}	2.72	2.68	9.67	150	3.576(4)
C32–H32···Cg(4)^{ii}	2.76	2.71	10.71	160	3.668(5)
C38–H38···Cg(7)^{iii}	2.88	2.74	17.75	143	3.683(4)
D–Cl···Cg	*D*–H	H···*A*	*D*···A	*D*–H···*A*	Cl···Cg
C5–Cl1···Cg(1)^{iv}	3.8215(15)	–3.688	15.18	72.43(15)	3.690(4)

Symmetry codes: (i) 1+*x*, *y*, *z*; (ii) 1–*x*, –*y*, 2–*z*; (iii) 3–*x*, 1–*y*, 2–*z*; (iv) –*x*, –*y*, 1–*z*.

3.757(4) Å; C17–H17···S1^{v} 3.674(4) Å; C17–H17···S2^{v} 3.728(4) Å; C20–H20···Cl1^{vi} 3.979(4) Å; C6–H6···Cl2^{vii} 3.796(4) Å; C24–H24···Cl2^{vii} 3.778(4) Å; C30–H30···N1^{iv} 3.569(4) Å; C18–H18···S1^{v} 3.647(4) Å; C26–H26···Cl2^{viii} 3.402(4) Å; Symmetry codes: (i) –1+*x*, –1+*y*,+*z*; (ii) 3–1–*x*, –*y*, 1–*z*; (iii) –1+*x*,+*y*,+*z*; (iv) 1+*x*,+*y*,+*z*; (v) 1–*x*, -*y*, 2–*z*; (vi) –*x*, –*y*, 1–*z*; (vii) 1–*x*, 1–*y*, 1–*z*; (viii) 2–*x*, 1–*y*, 1–*z*. Also, the crystal structure of each complex displays two different types of $\pi\cdots\pi$ stacking, edge-to-face of phenyl rings of ligands with distances in the range of 3.576–3.683 Å (Table 5), and slipped face-to-face of two phenyl rings with distances in the range of 4.097–5.868 Å (Table 6). The C–H···π edge-to-face (C38–H38···Cg7^{iii}) and $\pi\cdots\pi$ face-to-face interactions between the centers of gravity (Cg1···Cg3^{i}, Cg2···Cg3^{iii}, and Cg5···Cg7^{vi}) of the phenyl rings in molecular packing of *cis*-[Pt(L^4-S,O)$_2$] are shown in Figure 3. These stacking interactions direct the packing of the multilayer structure into a 3-D structure.

The dihedral angles between Pt1–S1–C8–N1–C1–O1 and Pt1–S2–C28–N3–C21–O2 planes, C15–C20 and C9–C14 planes are 4.34 and 81.13°, respectively (Figure 4). The unit cell and packing of the compound viewed approximately along the *c* axis is given in Figure 5. It can be said that there is a charge accumulation in the diagonals of the unit cell. There is intense electron localization available in the diagonal points. This is suitable for triclinic unit cell.

3.3. Antimicrobial activity studies

Safety tests, including cytotoxicity assays, are required for all products to be used in contact with humans. Cytotoxicity tests using culture cells have been accepted as a first step in identifying active compounds and for biosafety testing. Samples were placed in contact with a monolayer of HEp-2 cells and incubated. The cells were then scored for cytopathic effects [34, 35]. In the cytotoxicity assay, concentrations up to 1024 µg mL^{-1} of the compounds were not toxic for the replication HEp-2 cells. Thus, lower concentrations of all compounds (1000 µg mL^{-1}) were used for the experiments.

The *in vitro* biological activity of the four benzoyl thiourea derivative ligands (HL$^{1–4}$) and their Pt(II) complexes, *cis*-[Pt($L^{1–4}$-S,O)$_2$], were tested toward five type of bacteria and two types of fungal. The organisms used in the present investigations included *S. aureus* and *S. pneumoniae* (as Gram positive bacteria), *E. coli*, *P. aeruginosa* and *A. baumannii* (as Gram-negative bacteria) and *C. albicans* and *C. glabrata* (as fungal). The results of the biological activity of the synthesized compounds are recorded and compared with fluconazole (for fungal) and ampicillin (for bacteria) reference drugs. MIC values of the ligands and their Pt(II) complexes are listed in Table 1.

All free ligands and their Pt(II) complexes inhibited the growth of bacteria strains with MIC values ranging between 3.90 and 62.50 µg mL^{-1} (Table 1). When the synthesized Pt(II)

Table 6. Geometrical parameters of the π-stacking moieties involved in the $\pi\cdots\pi$ interaction for the *cis*-[Pt(L^4-S,O)$_2$] (Å, °).

Cg(I)[a]···Cg(J)	Distance	α[b]	γ[c]
Cg(1···Cg(3)^{i}	4.1148(19)	13	27.6
Cg(1)···Cg(7)^{ii}	4.8916(19)	68	83.7
Cg(1)···Cg(8)^{ii}	5.201(2)	65	43.7
Cg(2)···Cg(3)^{iii}	4.0970(19)	17	30.0
Cg(2)···Cg(7)*i*^{v}	5.600(2)	73	45.2
Cg(2)···Cg(8)^{ii}	5.358(2)	63	37.4
Cg(2)···Cg(8)^{iv}	5.2282(19)	63	82.8
Cg(3)···Cg(1)^{i}	4.1150(19)	13	33.2
Cg(3)···Cg(2)^{ii}	4.0970(19)	17	14.1
Cg(3)···Cg(3)^{i}	4.291(2)	0	34.6
Cg(3)···Cg(6)^{ii}	5.111(3)	16	37.4
Cg(3)···Cg(8)^{ii}	5.603(2)	67	89.3
Cg(4)···Cg(3)^{v}	5.714(3)	65	81.6
Cg(4)···Cg(3)^{i}	5.662(2)	65	61.6
Cg(4)···Cg(7)^{vi}	5.020(3)	87	87.8
Cg(5)···Cg(4)^{v}	4.694(2)	81	62.3
Cg(5)···Cg(4)^{iii}	5.520(2)	81	61.3
Cg(5)···Cg(5)^{vi}	4.516(2)	0	27.5
Cg(5)···Cg(7)^{vi}	4.417(2)	13	46.0
Cg(6)···Cg(3)^{iii}	5.111(3)	16	45.1
Cg(6)···Cg(4)^{vii}	5.241(3)	70	81.9
Cg(6)···Cg(7)^{iv}	5.481(2)	71	59.7
Cg(7)···Cg(2)^{iv}	5.600(2)	73	37.0
Cg(7)···Cg(4)^{iii}	5.682(2)	87	75.7
Cg(7)···Cg(5)^{vi}	4.417(2)	13	32.8
Cg(7)···Cg(6)^{iv}	5.481(2)	71	33.4
Cg(7)···Cg(8)^{v}	4.645(3)	87	56.4
Cg(7)···Cg(8)^{viii}	4.948(2)	87	78.0
Cg(8)···Cg(1)^{iii}	5.201(2)	65	35.0
Cg(8)···Cg(2)^{iii}	5.358(2)	63	34.5
Cg(8)···Cg(5)^{vii}	5.497(3)	89	63.8
Cg(8)···Cg(6)^{v}	5.947(2)	55	86.0
Cg(8)···Cg(7)^{v}	4.645(3)	87	59.0
Cg(8)···Cg(7)^{iv}	5.868(2)	87	83.2
Cg(1): Pt(1)–S(1)–C(8)–N(1)–C(1)–O(1)			
Cg(2): Pt(1)–S(2)–C(28)–N(3)–C(21)–O(2)			
Cg(3): C(2)–C(3)–C(4)–C(5)–C(6)–C(7)			
Cg(4): C(9)–C(10)–C(11)–C(12)–C(13)–C(14)			
Cg(5): C(15)–C(16)–C(17)–C(18)–C(19)–C(20)			
Cg(6): C(22)–C(23)–C(24)–C(25)–C(26)–C(27)			
Cg(7): C(29)–C(30)–C(31)–C(32)–C(33)–C(34)			
Cg(8): C(35)–C(36)–C(37)–C(38)–C(39)–C(40)			

Symmetry codes: (i) $-x, -y, 1-z$; (ii) $-1+x, y, z$; (iii) $1+x, y, z$; (iv) $2-x, 1-y, 2-z$; (v) x, y, z, (vi) $1-x, -y, 2-z$; (vii) $1+x, 1+y, z$; (viii) $3-x, 1-y, 2-z$.
[a]Cg(I): Center of gravity of ring I (= ring number in () above).
[b]Dihedral angle between planes I and J.
[c]Angle Cg(I)···Cg(J) vector and normal to plane J.

metal complexes compared with ampicillin, which is used as a reference drug, the synthesized complexes demonstrated lower activity against *S. aureus*, *S. pneumonia* (as Gram-positive bacteria) and *A. baumannii* (as Gram-negative bacteria). In contrast, the synthesized complexes showed mostly better activity than ampicillin against *E. coli* and *P. aeruginosa* (as Gram-negative bacteria). This may be explained by the differences between structures of bacterial cells [12, 55].

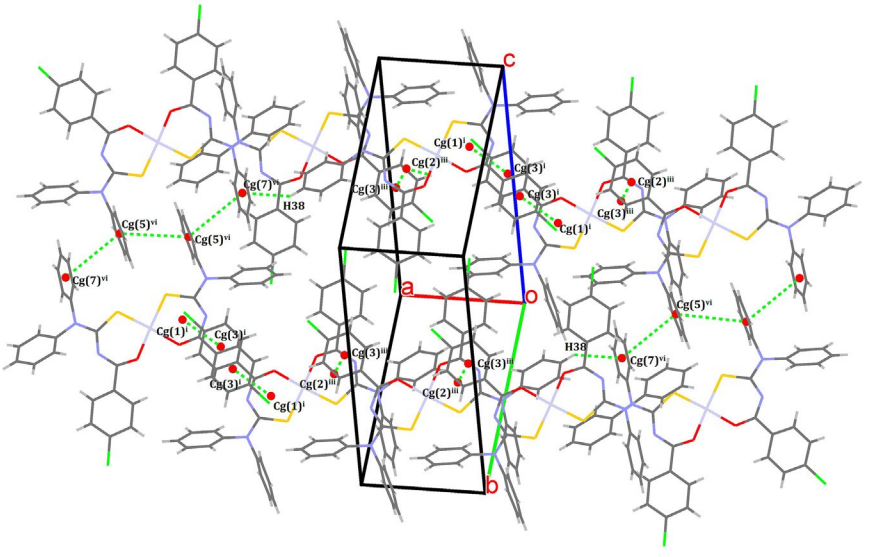

Figure 3. The molecular packing of *cis*-[Pt(L^4-S,O)$_2$] with the intermolecular interactions. The Cg–Cg ($\pi\cdots\pi$) and C–H$\cdots\pi$ (Cg) interactions (Symmetry codes: (i) $-x$, $-y$, $1-z$; (iii) $1+x$, y, z; (vii) $1+x$, $1+y$, z) are shown as green dashed lines.

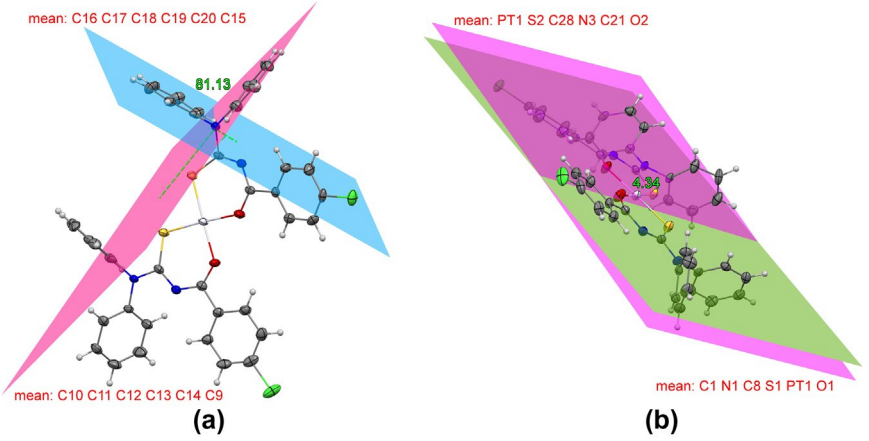

Figure 4. The dihedral angle between (a) Pt1–S1–C8–N1–C1–O1 and (b) Pt1–S2–C28–N3–C21–O2 (b) C15–C20 and C9–C14 planes.

HL^1 ligand displayed better activity than ampicillin used as reference drug against *E. coli* and *P. aeruginosa* bacteria with MIC values at 15.62 µg mL^{-1}. HL^2 ligand and its Pt(II) complex, *cis*-[Pt(L^2-S,O)$_2$], showed maximum inhibitory action against *P. aeruginosa* bacterium with MIC values at 7.80 and 3.90 µg mL^{-1}, respectively. They showed better activity than ampicillin, used as reference drug, against *P. aeruginosa* bacterium. HL^3 ligand exhibited the lowest activities against *E. coli* bacterium with MIC values at 125.00 µg mL^{-1} but its Pt(II) complex, *cis*-[Pt(L^3-S,O)$_2$], as effective as ampicillin used as reference drug against *E. coli* bacterium.

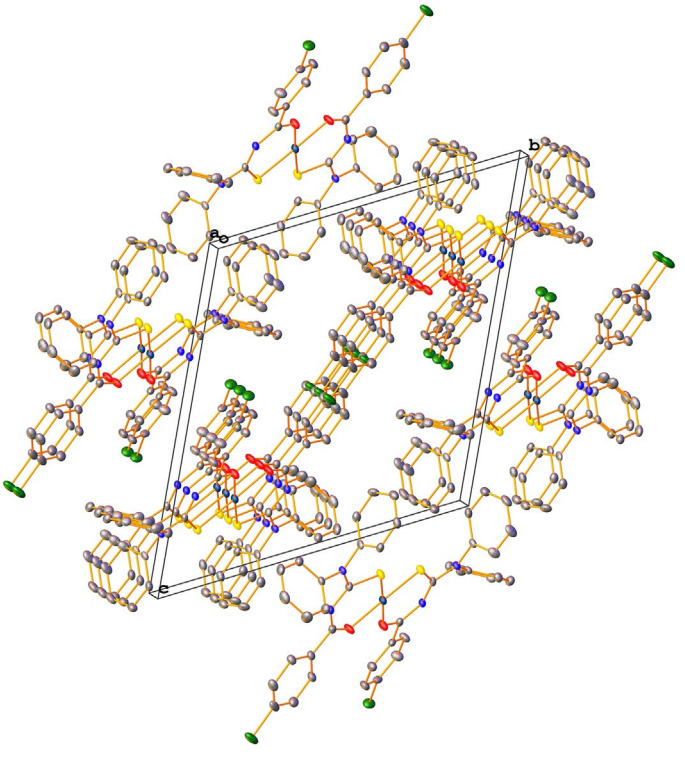

Figure 5. The unit cell and packing of *cis*-[Pt(L^4-S,O)$_2$] viewed approximately along the *c* axis.

HL^4 ligand and its Pt(II) complex, *cis*-[Pt(L^4-S,O)$_2$], are as effective as ampicillin reference drug against *E. coli* and *P. aeruginosa* bacteria with MIC values at 31.25 µg mL^{-1}. Among all the complexes, the *cis*-[Pt(L^2-S,O)$_2$] complex showed maximum inhibitory action against all bacterial strains with MIC values ranging between 3.90 and 15.62 µg mL^{-1} (Table 1).

All free ligands and their Pt(II) complexes inhibited the growth of fungal strains with MIC values ranging between 15.62 and 250.00 µg mL^{-1} but they are not as effective as fluconazole used as reference drug against all fungal strains. While all free ligands showed same activity against fungal with MIC values at 31.25 µg mL^{-1}, the *cis*-[Pt(L^1-S,O)$_2$] and *cis*-[Pt(L^3-S,O)$_2$] complexes exhibited best activity against *C. albicans* fungal with MIC values at 15.62 µg mL^{-1}.

According to data generated from this study, ligands and their Pt(II) complexes are observed to have different antimicrobial activity despite having similar structures. This is due to the fact that the zone of inhibition depends on both the diffusion of a compound into the agar medium and the solubility of compound. When the solubility is low, the diffusion is limited, resulting in the small zone, even for highly active derivatives presenting low MICs. On the other hand, high inhibition zone correlated with relatively high MIC could be explained by precipitation of a compound in the liquid medium and the changing of its real concentration [56]. Ligand HL^2 showed excellent inhibition against some bacteria species compared to other ligands. The structures of HL^1 through HL^3 vary gradually by increasing one carbon atom each. However, the antimicrobial results show significant different values for HL^2. In comparison to HL^1 and HL^2, HL^3, which has the longest carbon chain, could have

imitated the molecule in the lipid bilayer of organism and afforded less disruption in the bacteria membrane. Also, it is known that binding affinities (binding free energy) of compounds to micro-organisms through intermolecular interactions are effective on antimicrobial activity [57]. The increase of carbon chain in ligands can give rise to lesser binding affinity. Looking at the results obtained, we think that the binding affinity of HL^3 ligand to micro-organisms may be lower than that of the other two ligands [58, 59].

Moreover, antibacterial efficiency is higher than antifungal activity. Antimicrobial activity against bacteria may be due to the difference between cell structures of bacteria and fungi. While the cell walls of fungi contain chitin, the cell walls of bacteria contain murein [55]. The cell walls of fungi contain chitin, which enhance the rigidity and structural support. In addition, fungi contain ergosterol in cell membrane instead of cholesterol in the cell membrane of animals [9, 54, 60].

4. Conclusion

N,N-Di-*R*-*N*′-(4-chlorobenzoyl)thiourea type ligands and their Pt(II) complexes have been synthesized and characterized by elemental analysis, FTIR, ^{1}H, ^{13}C, cozy, and HMQC NMR studies. HL^2 ligand and *cis*-[Pt(L^4-S,O)$_2$] metal complex have been also characterized by a single-crystal X-ray diffraction study. The crystal data reveal that HL^2 crystallizes in space group $P2_1/n$ of the monoclinic crystal system while the *cis*-[Pt(L^4-S,O)$_2$] complex crystallizes in space group P-1 of the triclinic crystal system. The central Pt(II) atom is coordinated in *cis* form by two S and O donor atoms. The Pt(II) ion in complex has a slightly distorted square planar geometry. The analysis of crystal structures shows that intermolecular interactions have effective role in stabilization of crystal structure of both compounds. Synthesized compounds were tested *in vitro* against Gram-positive and Gram-negative bacteria and fungi. The evaluation of *in vitro* antimicrobial activities of compounds against various bacteria and fungi revealed that the HL^2 ligand and its platinum metal complex showed excellent inhibition against some bacteria species compared to other ligands and complexes. HL^2 and its platinum metal complex show best antimicrobial activity against *S. pneumoniae* as Gram-positive bacteria, *P. aeruginosa* and *A. baumannii* as Gram-negative bacteria. The activity of HL^2 became more pronounced when coordinated with the platinum ion. Hence, from all these observations, it was concluded that the *cis*-[Pt(L^2-S,O)$_2$] complex could be exploited for the design of novel antimicrobial drugs.

Supplementary material

Crystallographic data for the structures reported in this paper have been deposited at the Cambridge Crystallographic Data Center (CCDC) with quotation number CCDC-1532704 for HL^2 and CCDC-1532706 for *cis*-[Pt(L^4-S,O)$_2$], and can be obtained free of charge on application to CCDC 12 Union Road, Cambridge CB2 1EZ, U.K. [Fax: (internat.)+44(1223)336-033, E-mail: deposit@ccdc.cam.ac.uk].

Acknowledgments

We thank Dicle University Science and Technology Applied and Research Center (DUPTAM) for X-ray data collection. This academic work was linguistically supported by the Mersin Technology Transfer Office Academic Writing Center of Mersin University.

Disclosure statement

No potential conflict of interest was reported by the authors.

Funding

This work was supported by the Mersin University Research Fund [Project number 2015-AP4-1162].

ORCID

Ilkay Gumus http://orcid.org/0000-0002-9398-0057
Hakan Arslan http://orcid.org/0000-0003-0046-9442

References

[1] W. Henderson, B.K. Nicholson, M.B. Dinger, R.L. Bennett. *Inorg. Chim. Acta*, **338**, 210 (2002).
[2] R.C. Luckay, F. Mebrahtu, C. Esterhuysen, K.R. Koch. *Inorg. Chem. Commun.*, **13**, 468 (2010).
[3] A.F. Elhusseiny, A. Eldissouky, A.M. Al-Hamza, H.H.A.M. Hassan. *J. Mol. Struct.*, **1100**, 530 (2015).
[4] (a) L. Beyer, E. Hoyer, J. Liebscher, H. Hartmann. *Z. Chem.*, **21**, 81 (1981); (b) P. Muhl, K. Gloe, F. Dietze, E. Hoyer, L. Beyer. *Z. Chem.*, **26**, 81 (1986); (c) K.R. Koch. *Coord. Chem. Rev.*, **473**, 216 (2001).
[5] M. Iliş, M. Bucos, F. Dumitraşcu, V. Cîrcu. *J. Mol. Struct.*, **987**, 1 (2011).
[6] M.M. Habtu, S.A. Bourne, K.R. Koch, R.C. Luckay. *New J. Chem.*, **30**, 1155 (2006).
[7] J.C. Bruce, N. Revaprasadu, K.R. Koch. *New J. Chem.*, **31**, 1647 (2007).
[8] Y.F. Yuan, J.T. Wang, M.C. Gimeno, A. Laguna, P.G. Jones. *Inorg. Chim. Acta*, **324**, 309 (2001).
[9] Y.M. Zhang, T.B. Wei, L. Xian, L.M. Gao. *Phosphorus, Sulpher Silicon Relat. Elem.*, **179**, 2007 (2004).
[10] Y.M. Zhang, T.B. Wei, X.C. Wang, S.Y. Yang. *Indian J. Chem., Sect. B*, **37**, 604 (1998).
[11] W.Q. Zhou, B.L. Li, L.M. Zhu, J.G. Ding, Z. Yong, L. Lu, X.J. Yang. *J. Mol. Struct.*, **690**, 145 (2004).
[12] M. Eweis, S.S. Elkholy, M.Z. Elsabee. *Int. J. Biol. Macromol.*, **38**, 1 (2006).
[13] S. Saeed, M.H. Bhatti, M.K. Tahir, P.G. Jones. *Acta Crystallogr., Sect. E*, **64**, o1369 (2008).
[14] S. Saeed, N. Rashid, P.G. Jones, M. Ali, R. Hussain. *Eur. J. Med. Chem.*, **45**, 1323 (2010).
[15] N. Selvakumaran, S.W. Ng, E.R.T. Tiekink, R. Karvembu. *Inorg. Chim. Acta*, **376**, 278 (2011).
[16] N. Gunasekaran, S.W. Ng, E.R.T. Tiekink, R. Karvembu. *Polyhedron*, **34**, 41 (2012).
[17] S. Saeed, N. Rashid, P.G. Jones, M. Ali, R. Hussain. *Eur. J. Med. Chem.*, **45**, 1323 (2010).
[18] S. Hochreuther, R. Puchta, R. van Eldik. *Inorg. Chem.*, **50**, 8984 (2011).
[19] P. Jarzynka, A. Topolski, M. Uzarska, R. Czajkowski. *Inorg. Chim. Acta*, **413**, 60 (2014).
[20] S. Mihai, M. Negoiu. *Rev. Chim.*, **63**, 697 (2012).
[21] O.V. Dolomanov, L.J. Bourhis, R.J. Gildea, J.A.K. Howard, H. Puschmann. *J. Appl. Cryst.*, **42**, 339 (2009).
[22] L. Palatinus, G. Chapuis. *J. Appl. Cryst.*, **40**, 786 (2007).
[23] L. Palatinus, A. van der Lee. *J. Appl. Cryst.*, **41**, 975 (2008).
[24] L. Palatinus, S.J. Prathapa, S. van Smaalen. *J. Appl. Cryst.*, **45**, 575 (2012).
[25] G.M. Sheldrick. *Acta Crystallogr., Sect. C*, **71**, 3 (2015).
[26] A.L. Spek. *Acta Crystallogr., Sect. C*, **71**, 9 (2015).
[27] H. Arslan, U. Florke, N. Kulcu, E. Kayhan. *Turk. J. Chem.*, **30**, 429 (2006).
[28] G. Binzet, H. Arslan, U. Flörke, N. Külcü, N. Duran. *J. Coord. Chem.*, **59**, 1395 (2006).
[29] I. Gumus, U. Solmaz, O. Celik, G. Binzet, G.K. Balcı, H. Arslan. *Eur. J. Chem.*, **6**, 237 (2015).
[30] H. Arslan, D. Vanderveer, F. Emen, N. Kulcu. *Z. Krist-New Cryst. St.*, **218**, 479 (2003).
[31] G. Avşar, H. Arslan, H.-J. Haupt, N. Kulcu. *Turk. J. Chem.*, **27**, 281 (2003).
[32] F.G. Burlesson, T.M. Chambers, D.L. Wedbrauk. *Virology. A Laboratory Manual*, Academic Press, New York, NY (1992).
[33] National Committee for Clinical Laboratory Standards. *Reference Method for Broth Dilution Antifungal Susceptibility Testing of Yeasts. Approved Standard NCCLS Document M27-A*. National Committee for Clinical Laboratory Standards, Wayne, PA (2002).
[34] E. Borenfreund, J.A. Puerner. *J. Tissue Cult. Meth.*, **9**, 7 (1984).

[35] E. Borenfreund, J.A. Puerner. *Toxicol. Lett.*, **24**, 119 (1985).
[36] G.L. Woods, J.A. Washington, Antibacterial Susceptibility Tests: Dilution and Disk Diffusion Methods. In P.R. Murray, E.J. Baron, M.A. Pfaller, F.C. Tenover, R.H. Yolken (Eds), *Manual of Clinical Microbiology*, 6th Edn, American Society for Microbiology, Washington, DC, 1327 (1995).
[37] J.H. Jorgensen, M.J. Ferraro. *Clin. Infect. Dis.*, **26**, 973 (1998).
[38] N. Selvakumaran, N.S. Weng, R.T.E. Tiekink, R. Karvembu. *Inorg. Chim. Acta*, **376**, 278 (2011).
[39] B.O. Reilly, A.M. Plutin, H. Perez, O. Calderon, R. Ramos, R. Martinez, R.A. Toscano, J. Duque, H. Rodriguez-Solla, R. Martinez-Alvarez, M. Suarez, N. Martin. *Polyhedron*, **36**, 133 (2012).
[40] M. Oki. *Top. Stereochem.*, **14**, 1 (1983).
[41] D. Quiñonero, A. Frontera, M. Capó, P. Ballester, G.A. Suñer, C. Garau, P.M. Deyà. *New J. Chem.*, **25**, 259 (2001).
[42] R. Quintanilla-Licea, J.F. Colunga-Valladares, A. Caballero-Quintero, C. Rodríguez-Padilla, R. Tamez-Guerra, R. Gómez-Flores, N. Waksman. *Molecules*, **7**, 662 (2002).
[43] A. Rotondo, S. Barresi, M. Cusumano, E. Rotondo. *Polyhedron*, **45**, 23 (2012).
[44] A. Rotondo, S. Barresi, M. Cusumano, E. Rotondo, P. Donato, L. Mondello. *Inorg. Chim. Acta*, **410**, 1 (2014).
[45] K.R. Koch. *Coord. Chem. Rev.*, **216–217**, 473 (2001).
[46] M.K. Rauf, M. Ebihara, A. Badshah. *Acta Crystallogr., Sect. E*, **68**, o119 (2012).
[47] A.N. Mautjana, J.D.S. Miller, A. Gie, S.A. Bourne, K.R. Koch. *Dalton Trans.*, 1952 (2003).
[48] B.M. Yamin, U.M. Osman. *Acta Crystallogr., Sect. E*, **67**, o1286 (2011).
[49] W. Yang, W.Q. Zhou, Z.J. Zhang. *J. Mol. Struct.*, **828**, 46 (2007).
[50] H. Arslan, U. Flörke, N. Külcü, G. Binzet. *Spectrochim. Acta, Part A*, **68**, 1347 (2007).
[51] M.S. Yusof, R.H. Jusoh, W.M. Khairul, M.Y. Bohari. *J. Mol. Struct.*, **975**, 280 (2010).
[52] A.A. Al-Abbasi, B.M. Yamin, M.B. Kassim. *Acta Crystallogr., Sect. E*, **67**, 1891 (2011).
[53] A. Mohamadou, I. Déchamps-Olivier, J.P. Barbier. *Polyhedron*, **13**, 1363 (1994).
[54] H. Arslan, U. Florke, N. Kulcu. *Acta Chim. Slov.*, **51**, 787 (2004).
[55] G.H. Fleet. *Composition and Structure of Yeast Cell Walls: Current Topics in Medical Mycology*, Vol 1, Springer-Verlag, New York, NY, USA (1985).
[56] A. Bielenica, J. Stefańska, K. Stępień, A. Napiórkowska, E. Augustynowicz-Kopeć, G. Sanna, S. Madeddu, S. Boi, G. Giliberti, M. Wrzosek, M. Struga. *Eur. J. Med. Chem.*, **101**, 111 (2015).
[57] Y. He, Y. Wang, L. Tang, H. Liu, W. Chen, Z. Zheng, G. Zou. *J. Fluoresc.*, **18**, 433 (2008).
[58] M. Kvasnica, J. Oklestkova, V. Bazgier, L. Rarova, K. Berka, M. Strnad. *Steroids*, **85**, 58–64 (2014).
[59] M. Eweis, S.S. Elkholy, M.Z. Elsabee. *Int. J. Biol. Macromol.*, **38**, 1 (2006).
[60] G. Binzet, H. Arslan, U. Flörke, N. Külcü, N. Duran. *J. Coord. Chem.*, **59**, 1395 (2006).